2.1 DEVELOPMENT OF ODS FeCrAl FOR FUSION REACTOR APPLICATIONS – B. A. Pint, K. A. Unocic, S. Dryepondt and D. T. Hoelzer (Oak Ridge National Laboratory, USA)

OBJECTIVE

The dual coolant lead-lithium (DCLL) blanket concept requires improved Pb-Li compatibility with ferritic steels in order to demonstrate viable blanket operation in a DEMO-type fusion reactor. The goal of this work is to develop an oxide dispersion strengthened (ODS) alloy with improved compatibility with Pb-Li and excellent mechanical properties. The current focus is characterizing the performance of a group of ODS alloys based on Fe-12Cr-5Al.

SUMMARY

Four experimental ODS FeCrAl heats of composition Fe-12Cr-5Al were prepared by mechanical alloying with additions of Y_2O_3, Y_2O_3 + ZrO_2, Y_2O_3 + HfO_2 and Y_2O_3 + TiO_2. Characterization of the as-extruded and aged microstructures are in progress and are compared to a commercial ODS FeCrAl alloy, PM2000. An initial Pb-Li compatibility evaluation was performed at 700°C on the first three alloys. The fourth alloy with TiO_2 was recently produced and tensile properties have been measured from 25° to 800°C. This alloy had high strength but low ductility at 25° and 400°C consistent with its high hardness. Initial creep testing has begun on the alloy with HfO_2 at 800°C and 100 MPa.

PROGRESS AND STATUS

Introduction

The DCLL blanket concept (Pb-Li and He coolants) is the leading U.S. design for a test blanket module (TBM) for ITER and for a DEMO-type fusion reactor.[1] With reduced activation ferritic-martensitic (FM) steel as the structural material, the DCLL is limited to ~475°C metal temperature because Fe and Cr readily dissolve in Pb-Li above 500°C and Eurofer 97 plugged a Pb-Li loop at 550°C.[2-3] For a higher temperature blanket for DEMO, structural materials with enhanced creep and compatibility are needed. ODS FeCrAl alloys are one possibility to meet this objective and considerable research on ODS FeCr alloys has shown an excellent combination of creep strength and radiation resistance.[4-7] However, these ODS FeCr alloys do not have adequate compatibility with Pb-based coolants, such as Pb-Bi eutectic (LBE) [8-11]. With the addition of Al, isothermal compatibility tests have shown low mass losses at up to 800°C.[12] Therefore, a materials development effort is underway, specific to this application. ODS FeCrAl was commercialized in the 1970's for its high temperature (>1000°C) creep and oxidation resistance [13] and other research groups are currently investigating new FeCrAl alloy compositions for fission and fusion applications with liquid metals.[14-16]

Previous initial work [17-19] had identified Fe-12wt.%Cr-5Al as a target composition with low Cr to minimize α' formation during irradiation [20], while maintaining 5%Al for Pb-Li compatibility.[17,21] Using diffusion couples, combinations of oxides also were identified that could form stable ternary compounds. The properties of this first generation composition are being measured with a second generation being designed based on this information.

Experimental Procedure

Four experimental ODS FeCrAl ferritic alloys were produced by mechanical alloying (MA). Powder of

specified composition Fe-12.1wt.%Cr-5.0Al and particle size range ~45-150 μm was prepared by Ar gas atomization by ATI Metal Powders. The FeCrAl powder was blended with 0.3%Y_2O_3 powder (17-31 nm crystallite size, produced by Nanophase, Inc.) and subsequent 1kg batches included additions of 0.4ZrO_2, 0.22HfO_2 and 0.2TiO_2 powders (<100 nm diameter from American Elements). Each batch was ball milled for 40 h in Ar gas atmosphere using the Zoz CM08 Simoloyer ball mill. After ball milling, the powders were placed in mild steel cans, degassed at 300ºC under vacuum and sealed. The cans were equilibrated at 950ºC for 1 h and then extruded through a rectangular shaped die. Table 1 shows the as-extruded compositions of each alloy. The alloys with additional ZrO_2, HfO_2 and TiO_2 oxide additions showed higher O contents and the Cr and Al contents were lower than the starting powder. Other typical impurities were Co, Cu, Ni and Mn at the 0.01-0.02% level and the C and N pickups from the milling process were acceptable. Tensile tests were performed using SS-3 type tensile specimens fabricated with the gage section (7.62 mm long and 0.762 mm thick) parallel to the extrusion axis of the ODS FeCrAl heats. The tensile tests were conducted in an MTS hydraulic frame at temperatures ranging from 25ºC-800ºC and a strain rate of 10^{-3} s^{-1}. Creep tests were performed at 800°C on similar size specimens with a 2 x 2 mm gage section.

Static Pb-Li capsule tests were performed using Mo (inert to Pb-Li) inner capsules and type 304 stainless steel (SS) outer capsules to protect the inner capsule from oxidation. The ODS FeCrAl specimens were ~1.5 mm thick and 4-5 cm^2 in surface area with a 600 grit surface finish and were held with 1 mm diameter Mo wire. The capsules were loaded with 125 g of Pb-Li in an Ar-filled glove box. The Pb-Li was melted and cast at ORNL and had Li contents of 15.6-16.5 at%. The Mo and SS capsules were welded shut to prevent the uptake of impurities during the isothermal exposure. After exposure, residual Pb-Li on the specimen surface was removed by soaking in a 1:1:1 mixture of acetic acid, hydrogen peroxide and ethanol for up to 72 h. Mass change was measured with a Mettler-Toledo balance with an accuracy of 0.01 mg/cm^2. Post-test specimen surfaces were examined using x-ray diffraction (XRD) and secondary electron microscopy (SEM) equipped with energy dispersive x-ray (EDX) analysis. After surface characterization, the specimens were metallographically sectioned and polished and examined by light microscopy, SEM and electron probe microanalysis (EPMA) using wavelength dispersive x-ray analysis.

The as-extruded and aged microstructure was characterized using a Hitachi S4800 Field Emission Gun (FEG) Scanning Electron Microscope (SEM) equipped with X-ray Energy Dispersive Spectroscopy (XEDS). Specimens for Transmission Electron Microscope (TEM) analysis were prepared by Focused Ion Beam (FIB, Hitachi model NB500) using the in-situ lift-out method from the polished specimens. A Philips model CM200 FEG-TEM/STEM (Scanning TEM) with XEDS and EELS (Electron Energy Loss Spectroscopy) was used for analysis. Bright-Field (BF) and High Angle Annular Dark Field (HAADF) STEM and Energy Filtered TEM (EFTEM) imaging methods were used in the microstructural investigations. For high resolution imaging a JEOL 2200FS-AC FEG STEM 200kV probe corrected microscope (using CEOS Cs-Corrector) was used that has 0.7Å resolution in STEM mode equipped with a Bruker XFlash® 6|30 silicon drift detector (SDD) that combines excellent energy resolution with the larger solid angle of a 30 mm^2 active chip area. Electron diffraction patterns and fast Fourier transform (FFT) were used for phase identification. Vickers hardness was measured using a 200 or 500g load.

Table 1. Alloy chemical compositions (mass% or ppmw) by inductively coupled plasma analysis and combustion analysis.

Material	Fe%	Cr%	Al%	Y%	O	C	N	S	Other
Powder	82.8	12.1	5.0	<	64	31	11	<3	0.004Si
125Y	83.3	11.4	4.8	0.19	842	380	455	20	0.05W, 0.02Si, 0.01Ti
125YZr	82.8	11.5	4.9	0.18	1920	250	161	10	0.30Zr, 0.01Hf, 0.01Si
125YHf	82.3	11.7	4.8	0.17	2280	220	110	10	0.68Hf, 0.01Zr, 0.01Si
125YTi	82.4	12.0	4.9	0.16	2220	350	135	30	0.20Ti,0.01Si
PM2000	74.1	19.1	5.5	0.39	2480	14	86	8	0.48Ti, 0.02Si

< indicates below the detectability limit of <0.01%

Results and Discussion

Previously the general microstructure features were reported such as average grain size and the oxide precipitate size distribution of the new ODS alloys.[19] In the first three alloys characterized, a high number density of small (~3nm) particles were distributed uniformly throughout the matrix and showed dark contrast relative to the surrounding matrix in HAADF STEM images. The current work is focused on identifying the oxide phases that formed in the as-extruded 125YZr with Y_2O_3 + ZrO_2 (Figure 1) and 125YHf with Y_2O_3 + HfO_2 (Figure 2) alloys and the latter alloy after thermal ageing (Figure 3) using high resolution TEM techniques. In 125YZr, a few large bright contrast particles were observed that contained only Zr. These precipitates were identified as ZrO using a combination of EDS and FFT analyses (Figure 1) from which interplanar spacing and angles were measured and compared with the JCPDS values. The formation of metastable ZrO suggests the as-extruded structure is not at equilibrium. In as-extruded 125YHf, a trimodal particle size distribution was observed and phase identification is still in progress with examples shown in Figure 2. After ageing at 1000°C for 1 and 100 h, both the bright Hf-rich particles and the dark Al-rich oxides appeared to coarsen, Figure 3. The particles with mixed dark and bright areas began to disappear and small Y+Hf oxides appeared (EDS maps associated with Figure 3d).

Ageing experiments were conducted on all of the alloys at 800°, 1000° and 1200°C. However, it was not feasible to perform TEM after all conditions. Therefore, hardness was used as an indication of the microstructure stability. Figure 4 summarizes the measurements made at 800° and 1000°C with

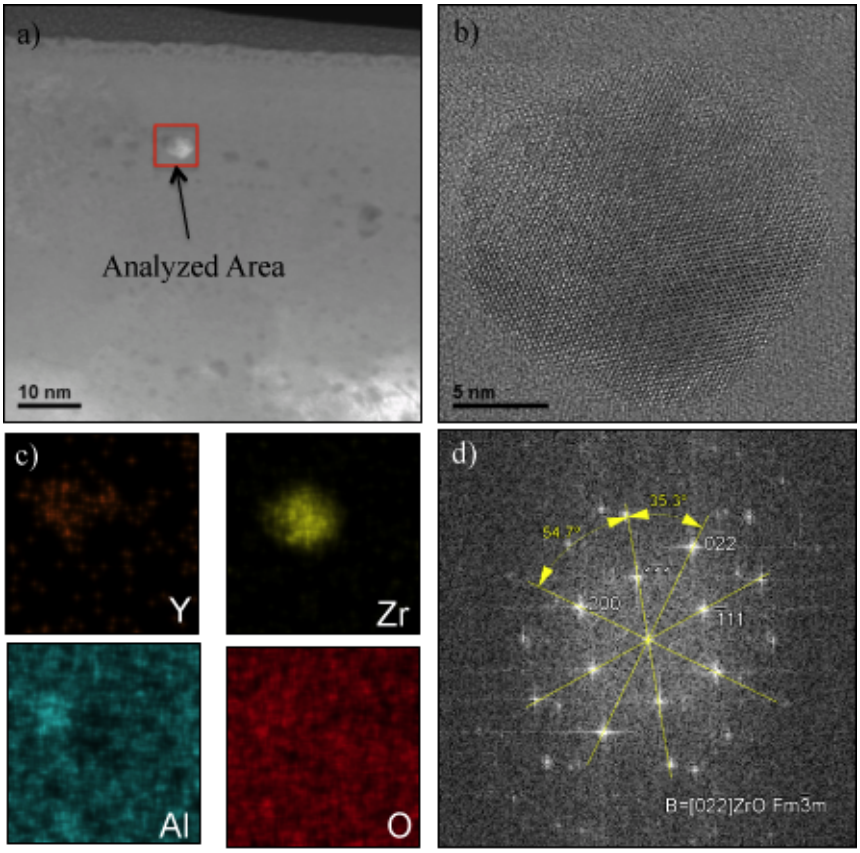

Figure 1. a) HAADF image of the 125YZr as-extruded (lift-out FIB) microstructure. b) High resolution BF-STEM of the Zr-rich particle (from the area marked in 1a) identified using c) EDS Map and d) FFT as ZrO.

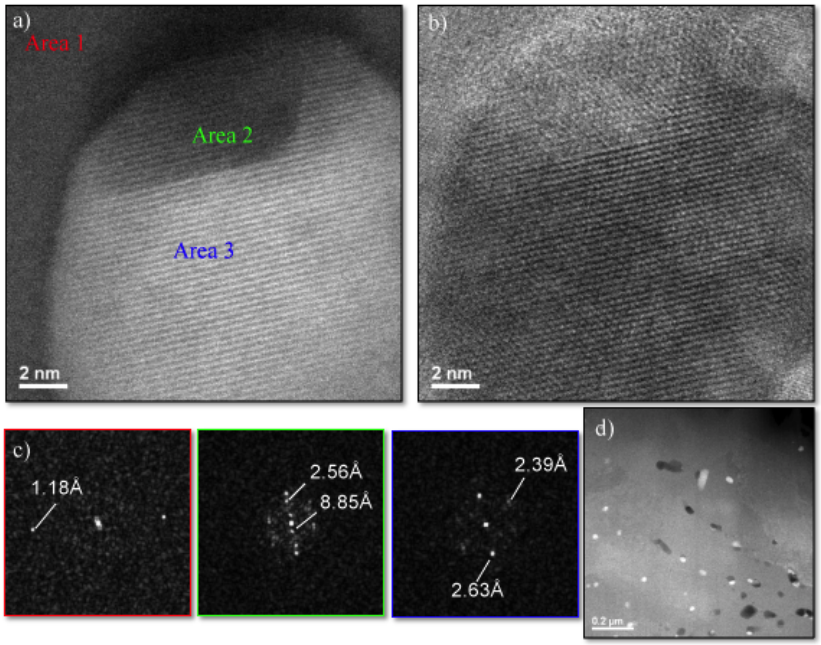

Figure 2. High resolution (a) HAADF and b) BF-STEM images of a typical "double" particle from 125YHf after extrusion with c) FFT and d) low magnification HAADF image showing the microstructure.

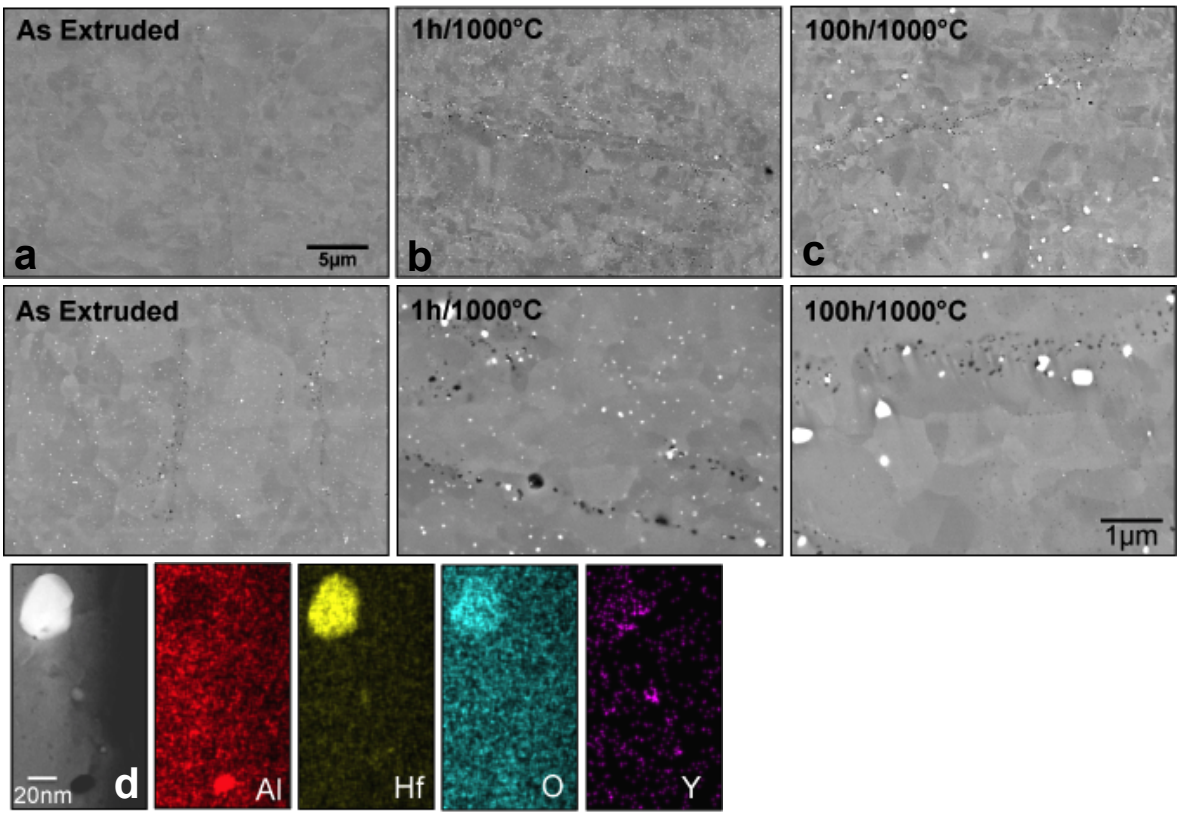

Figure 3. SEM backscattered electron images of 125YHf, a) as-extruded, b) after 1 h at 1000°C, and c) 100 h at 1000°C at two magnifications. The Hf-rich (bright) and Al-rich (dark) particles coarsen with exposure time. (d) HAADF image with associated XEDS Al, Hf, O and Y maps from area in (c).

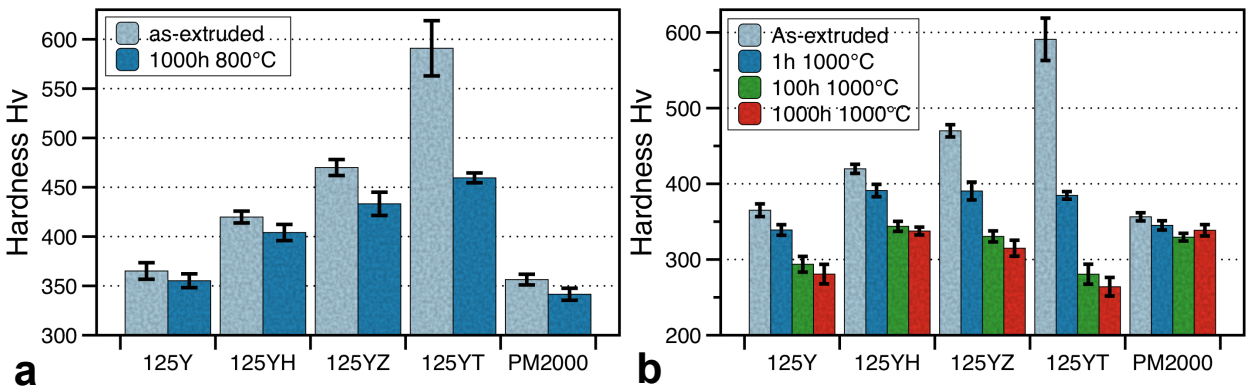

Figure 4. Vickers hardness values as a function of aging time at (a) 800°C and (b) 1000°C.

unrecrystallized PM2000 used as a comparison. While the alloy with Y_2O_3 + TiO_2 had the highest starting hardness, it also experienced a large drop after annealing at both 800° and 1000°C. After 1000h at 1000°C, it had the lowest hardness of any of the alloys. The other ODS alloys experienced relatively small decreases in hardness after 1000h at 800°C, and larger drops after annealing at 1000°C. There was little statistical difference between the hardness values measured after 100 and 1000 h at 1000°C, suggesting that the microstructures had stabilized. Based on these hardness measurements, PM2000 showed the highest microstructural stability. The as-extruded hardness for PM2000 was relatively low but the decrease after annealing was relatively minor at both temperatures. The hardness measurements at 1200°C are in progress.

The mass change data for the new ODS alloys after 1000 h at 700°C in static Pb-Li is summarized in Figure 5.[22] For reference, the mass change for several cast FeCrAl alloys [21] is shown as well as commercial ODS FeCrAl alloy, PM2000, Table 1. When Al was present in the alloy, a $LiAlO_2$ layer

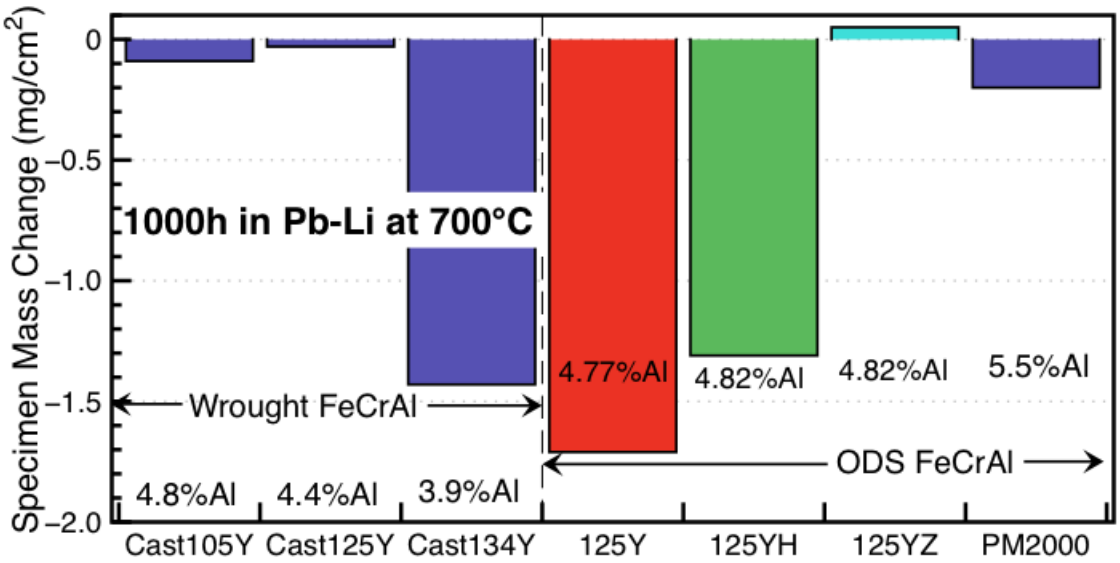

Figure 5. Specimen mass change for alloy specimens exposed for 1000h at 700°C in static Pb-Li.

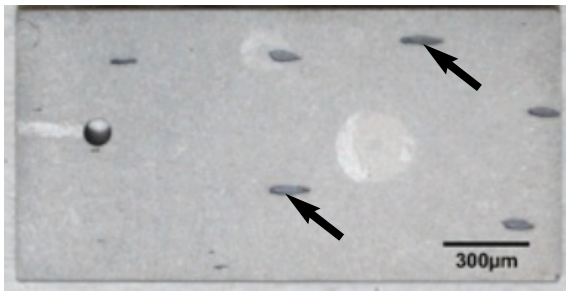

Figure 6. Light microscopy of the 125Y specimen after 1000 h in Pb−Li at 700°C with arrows pointing to the large surface pits.

(identified by XRD) formed on each specimen [12,23] from O impurities in the Pb-Li (200-400ppmw as cast) and this layer inhibited dissolution of the alloy into the liquid metal. The high mass loss for the Y_2O_3 specimen (125Y) was linked to ~300µm deep pits in the surface (arrows in Figures 6 and 7a), which suggested that powder with little or no Al was incorporated in this first batch of ball milled material and was selectively dissolved from the specimen. Similar extreme behavior was observed when an aluminized 9Cr steel specimen was exposed with one cut (uncoated) face [24]. Both Fe and Cr have a high solubility in Pb-Li and without the Al to form a stable oxide, dissolution occurred rapidly without the liquid reaching saturation thereby slowing the dissolution rate. Surprisingly, the Y_2O_3 + HfO_2 specimen (125YH) also showed similar mass loss as the 125Y specimen. There was no indication of significant dissolution but spallation near the specimen edges was observed. The Y_2O_3 + ZrO_2 specimen (125YZ) showed the lowest mass change, which was consistent with the cast FeCrAl alloys of similar composition, Figure 5. The higher mass loss for the cast alloy with only 4 wt.%Al indicated that the Al content could not be reduced below ~5wt.%Al for this application. Figure 7 shows cross-sections of each of the new ODS alloys exposed with little observable difference between the specimens with HfO_2 and ZrO_2. Further characterization using EPMA, found some Al depletion in the substrate with a small Al gradient measured ~75µm beneath the surface, but similar for all of the materials, Figure 8. The depletion of 0.5-1at%Al near the surface is more than had been observed previously for PM2000 exposed for the same conditions.[12] The most severe depletion was observed beneath one of the surface pits (Figure 6 or 7a). A Pb-Li exposure for a specimen of the Y_2O_3 + TiO_2 alloy is in progress.

Figure 9 summarizes all of the tensile data for this group of alloys, with the recent addition of the data for

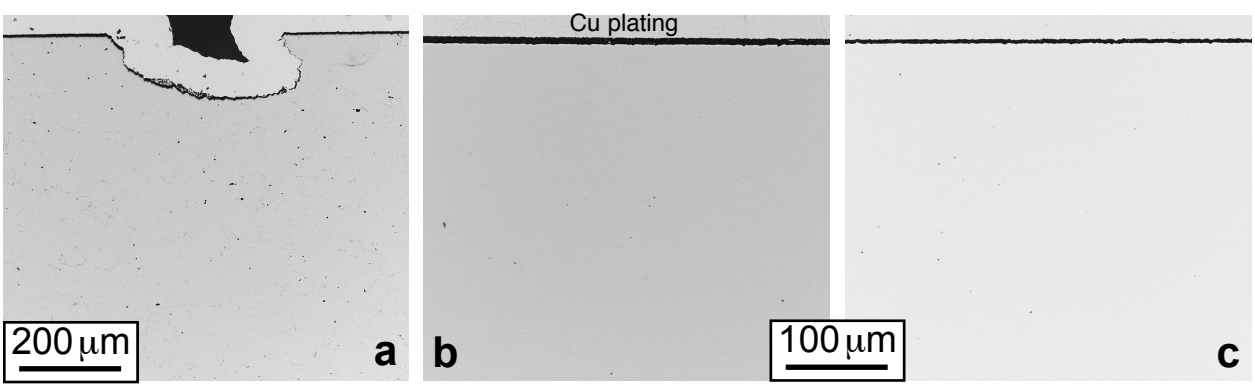

Figure 7. Light microscopy of polished cross-sections after 1000 h in Pb-Li at 700°C of (a) 125Y, (b) 125YHf and (c) 125YZr.

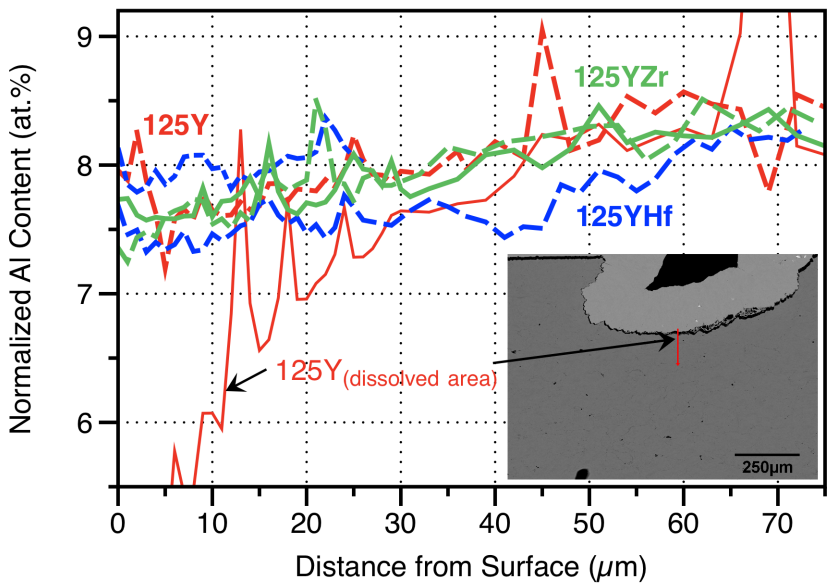

Figure 8. EPMA Al composition profiles from the alloy beneath the surface oxide formed after 1000 h at 700°C in Pb-Li. Two profiles are shown for each ODS alloy.

the alloy with Y_2O_3 + TiO_2. The results are compared to data for unrecrystallized PM2000. This material had the highest yield stress (σ_{ys}) and ultimate tensile strength (σ_{uts}) at 25°-600°C but also showed lower ductility at 25° and 400°C. Measurement of the tensile properties after ageing is in progress.

The alloy with Y_2O_3 + HfO_2 was selected for creep studies at 800°C and 100 MPa. The first creep test showed an initial drop in strain, likely due to a measurement error. After the rate had stabilized, the stress was increased to 120 MPa but the specimen then failed after < 50h. This suggested that 100 MPa was

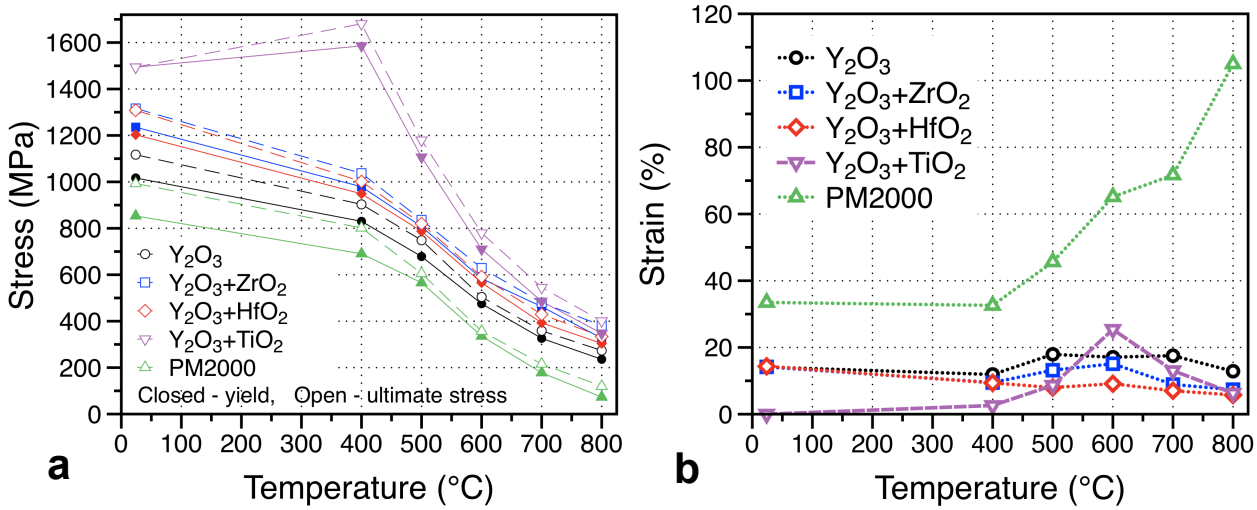

Figure 9. Tensile properties of the ODS FeCrAl heats as a function of test temperature. (a) yield stress and ultimate tensile strength and (b) total elongation.

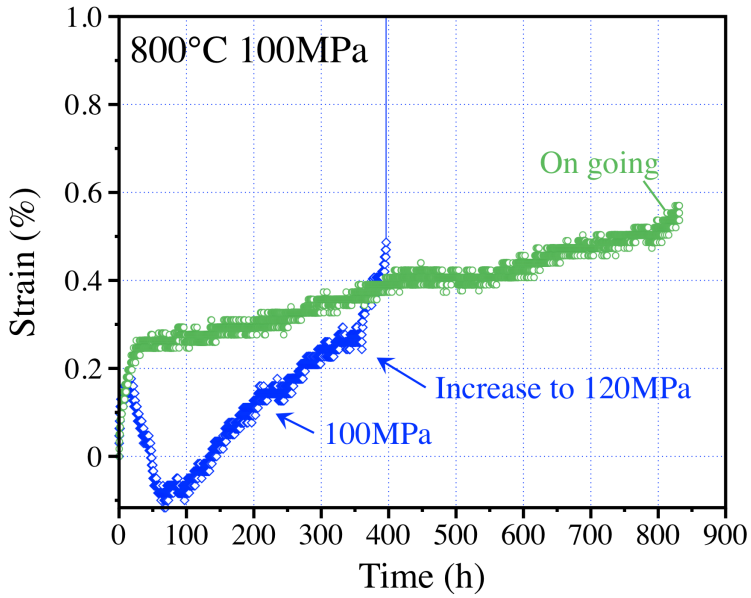

Figure 10. Strain as a function of exposure time for two 125YHf specimens tested at 800°C/100 MPa.

near the threshold stress for this alloy at 800°C. A second creep test at 800°C/100 MPa is in progress with steady behavior past 800 h. Additional testing will be conducted on unrecrystallized PM2000 and the Y_2O_3 + ZrO_2 alloy for comparison.

References

[1] M. Abdou, D. Sze, C. Wong, M. Sawan, A. Ying, N. B. Morley and S. Malang, Fus. Sci. Tech., 47 (2005) 475.
[2] O. K. Chopra, D. L. Smith, P. F. Tortorelli, J. H. DeVan and D. K. Sze, Fusion Technol., 8 (1985) 1956.
[3] J. Konys, W. Krauss, J. Novotny, H. Steiner, Z. Voss and O. Wedemeyer, J. Nucl. Mater. 386-88 (2009) 678.
[4] S. Ukai and M. Fujiwara, J. Nucl. Mater. 307 (2002) 749.
[5] G. R. Romanowski, L. L. Snead, R. L. Klueh, D. T. Hoelzer, J. Nucl. Mater., 283-287 (2000) 642.
[6] R. L. Klueh, J. P Shingledecker, R. W. Swindeman, D. T. Hoelzer, J. Nucl. Mater. 341 (2005) 103.
[7] D. A. McClintock, M. A. Sokolov, D. T. Hoelzer and R. K. Nanstad, J. Nucl. Mater., 392 (2009) 353.
[8] T. Furukawa, G. Müller, G. Schumacher, A. Weisenburger, A. Heinzel and K. Aoto, J. Nucl. Mater. 335 (2004), 189.
[9] P. Hosemann, H.T. Thau, A.L. Johnson, S.A. Maloy and N. Li, J. Nucl. Mater. 373 (2008) 246.
[10] C. Schroer, J. Konys, T. Furukawa and K. Aoto, J. Nucl. Mater. 398 (2010) 109.
[11] A. Weisenburger, K. Aoto, G. Müller, A. Heinzel, G. Schumacher and T. Furukawa, J. Nucl. Mater. 358 (2006) 69.
[12] B. A. Pint, L. R. 122012) 129.
[13] J. D. Whittenberger, Met. Trans. 9A (1978) 101.
[14] J. Lim, H.O. Nam, I.S. Hwang and J.H. Kim, J. Nucl. Mater. 407, (2010), 205.
[15] A. Kimura, et al., J. Nucl. Mater. 417, (2011), 176.

[16] S. Takaya, et al., J. Nucl. Mater. 428, (2012), 125
[17] B. A. Pint, D. T. Hoelzer, D. Shin, J. O. Kiggans, Jr., K. A. Unocic, DOE/ER-0313/53 (2012) 10.
[18] B. A. Pint, D. T. Hoelzer and K. A. Unocic, DOE/ER-0313/54 (2013) 27.
[19] D. T. Hoelzer, K. A. Unocic, S. Dryepondt and B. A. Pint, DOE/ER-0313/55 (2013) 5.
[20] C. Capdevila, M.K. Miller, K.F. Russell, J. Chao, J.L. González-Carrasco, Mater. Science and Engineering A, 490, (2008), 277.
[21] K. A. Unocic and B. A. Pint, J. Nucl. Mater. in press.
[22] K. A. Unocic, D. T. Hoelzer and B. A. Pint, Mater. High Temp. in press.
[23] B. A. Pint and K. L. More, J. Nucl. Mater. 376 (2008) 108.
[24] B. A. Pint and K. A. Unocic, J. Nucl. Mater. 442 (2013) 572.